Supporting Materials

Dissecting the collective cell behaviors in polarization and alignment on micropatterned substrate

Shijie He, Chenglin Liu, Xiaojun Li, Shaopeng Ma, Bo Huo, Baohua Ji

Contents

S1. Derivation of equilibrium equation of cell layer

Consider the equilibrium of an infinitesimal element of the ring-like cell layer shown in Fig. S1A. The free-body diagram of the infinitesimal element is illustrated in Fig. S1 B (top view) and S1 C (side view).

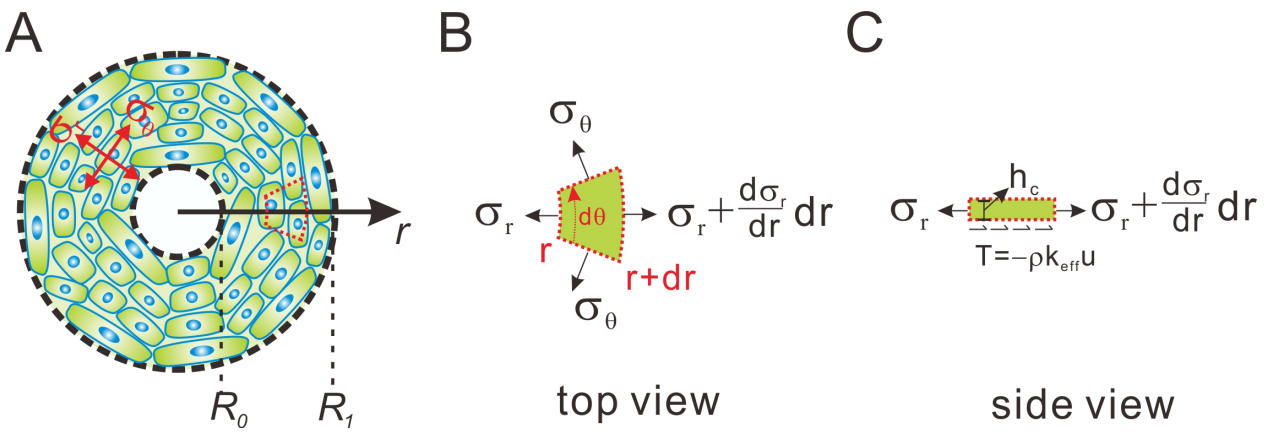

Figure S1. Free body diagram of the element in cell layer

Because of symmetry of the cell layer, we only need to consider the equilibrium of the element in radial direction. According to the illustration in the side view of the element, the equilibrium of the element in radial direction should satisfy

$$\left(\sigma_r+\frac{d\sigma_r}{dr}dr\right)(r+dr)d\theta h_c-\sigma_r r d\theta h_c-2\sigma_\theta \sin\left(\frac{d\theta}{2}\right)dr h_c+T\frac{rd\theta+(r+dr)d\theta}{2}dr=0 \qquad \text{(s1.1)}$$

where $T=-k_{eff}\rho u$ is the cell-matrix interaction, i.e., the traction stress. Because $d\theta$ is infinitesimal, $\sin(d\theta/2)=d\theta/2$. Neglecting the higher order infinitesimal terms of $d\theta$ and dr, Eq. (s1.1) is simplified into

$$\frac{d\sigma_r}{dr}+\frac{\sigma_r-\sigma_\theta}{r}+\frac{T}{h_c}=0 \qquad (3)$$

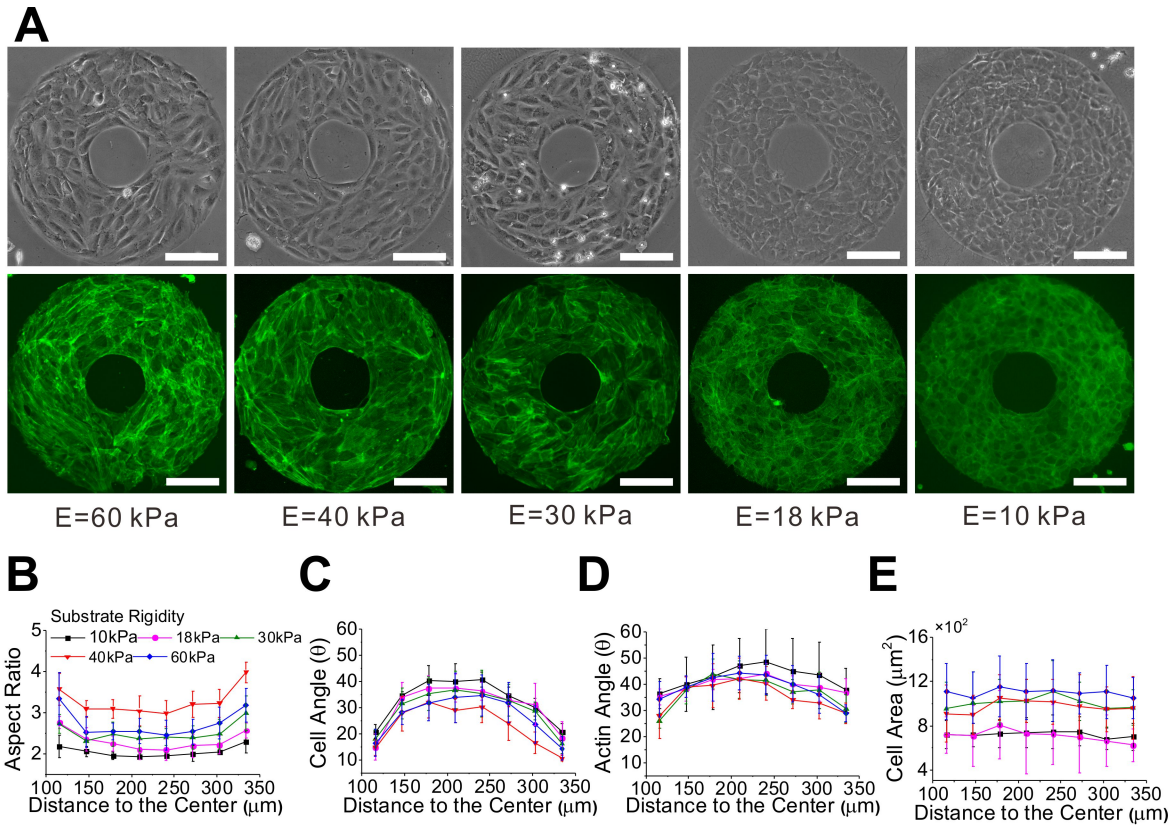

Figure S2. Cell polarization and alignment on a ring pattern of different stiffnesses. (A) Phase contrast images of cell morphology and alignment, and associated fluorescence images of actin on the ring pattern of five different stiffnesses, i.e. 60kPa, 40kPa, 30kPa, 18kPa and 10kPa; Scale bars =200μm; (B) The mean aspect ratio of cells versus the distance of cell to the center of the ring pattern; (C) The mean cell angle as function of the distance of cell to the center of ring; (D) The alignment of actin as function of the distance of cell to the center of ring. (E) The mean cell area as function of the distance of cell to the ring center.

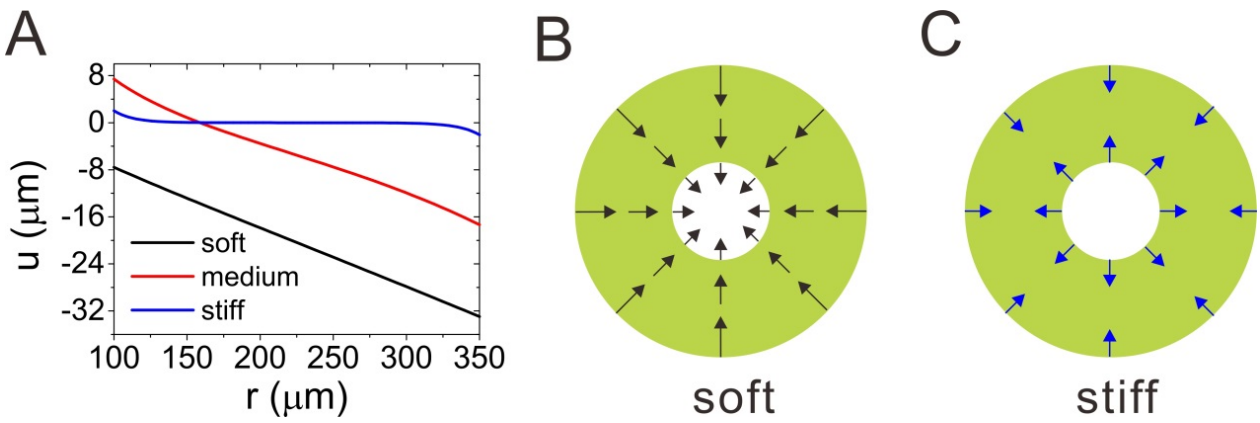

Figure S3. The distribution of deformation in cell layer changing with the stiffness of substrate

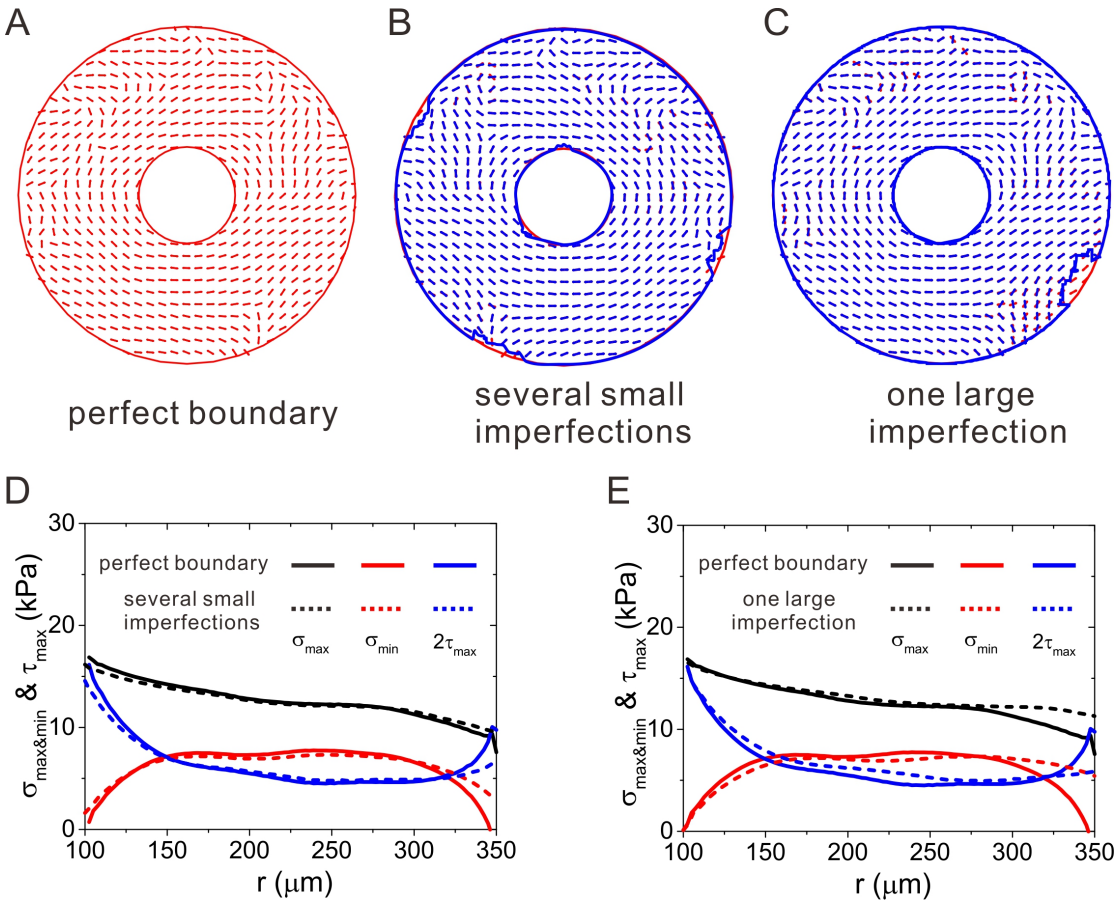

Figure S4. The effect of the imperfections of pattern edge on the reconstructions of the in-plane stresses. A) Cell layer with perfect boundary; (B) Cell layer with multiple small imperfections at the boundary; (C) Cell layer with one large imperfection; Vectorial representation of the in-plane maximum principal stress on the perfect cell layer (A), and its comparison with the direction of the maximum principal stress on the cell layer having several small imperfections (B) and that having one large imperfection (C). (D) and (E) show the comparison of magnitude of the principal stresses (maximum & minimum) and the maximum shear stress between the perfect cell layer and that with imperfections of the two kinds, respectively.

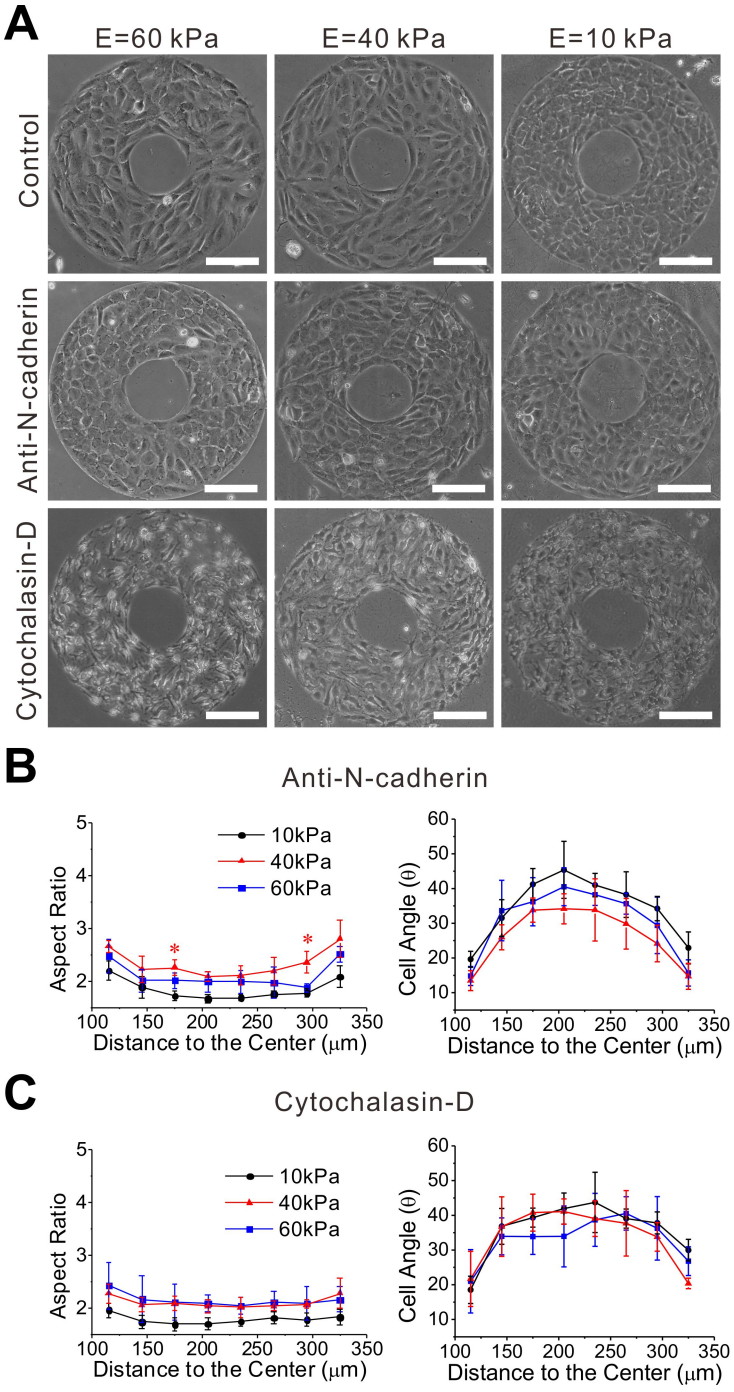

Figure S5. The perturbation of adhesions and contractility of cells impaired the biphasic dependence of polarization and alignment of cells on stiffness of substrate. (A) Phase contrast images of the cell layer on the ring pattern for the cases of control, treatment by Anti-N-cadherin and treatment by cytochalasin-D for three typical stiffness of substrate, 10kPa, 40kPa and 60kPa.

(B) Anti-N-cadherin treatment significantly weakened the biphasic dependence of aspect ratio, and caused the biphasic behaviors of cell angle to disappear with no statistical significance. C) Cytochalasin-D treatment brought more severe perturbation and thus destroyed the biphasic behaviors of aspect ratio and cell angle completely.

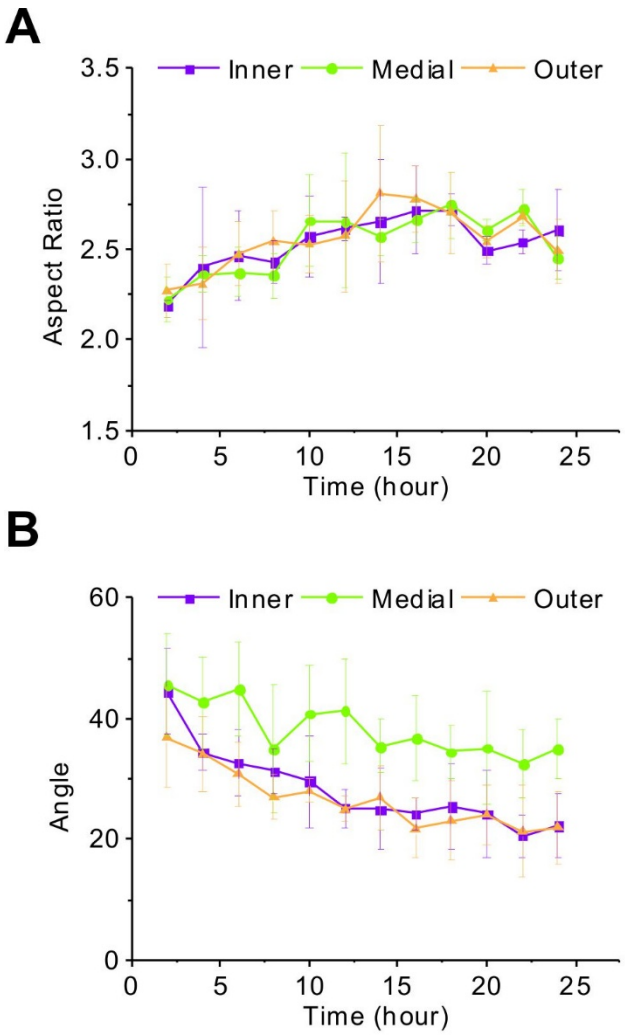

Figure S6. Time evolution of cell arrangement and polarization on ring pattern (inner radius 100μm) during the period of 24-hour of cell seeding/culture. (A) The evolution of aspect ratio of cell. (B) The evolution of cell orientation denoted by the cell angle with respect to the direction of the maximum principle stress.

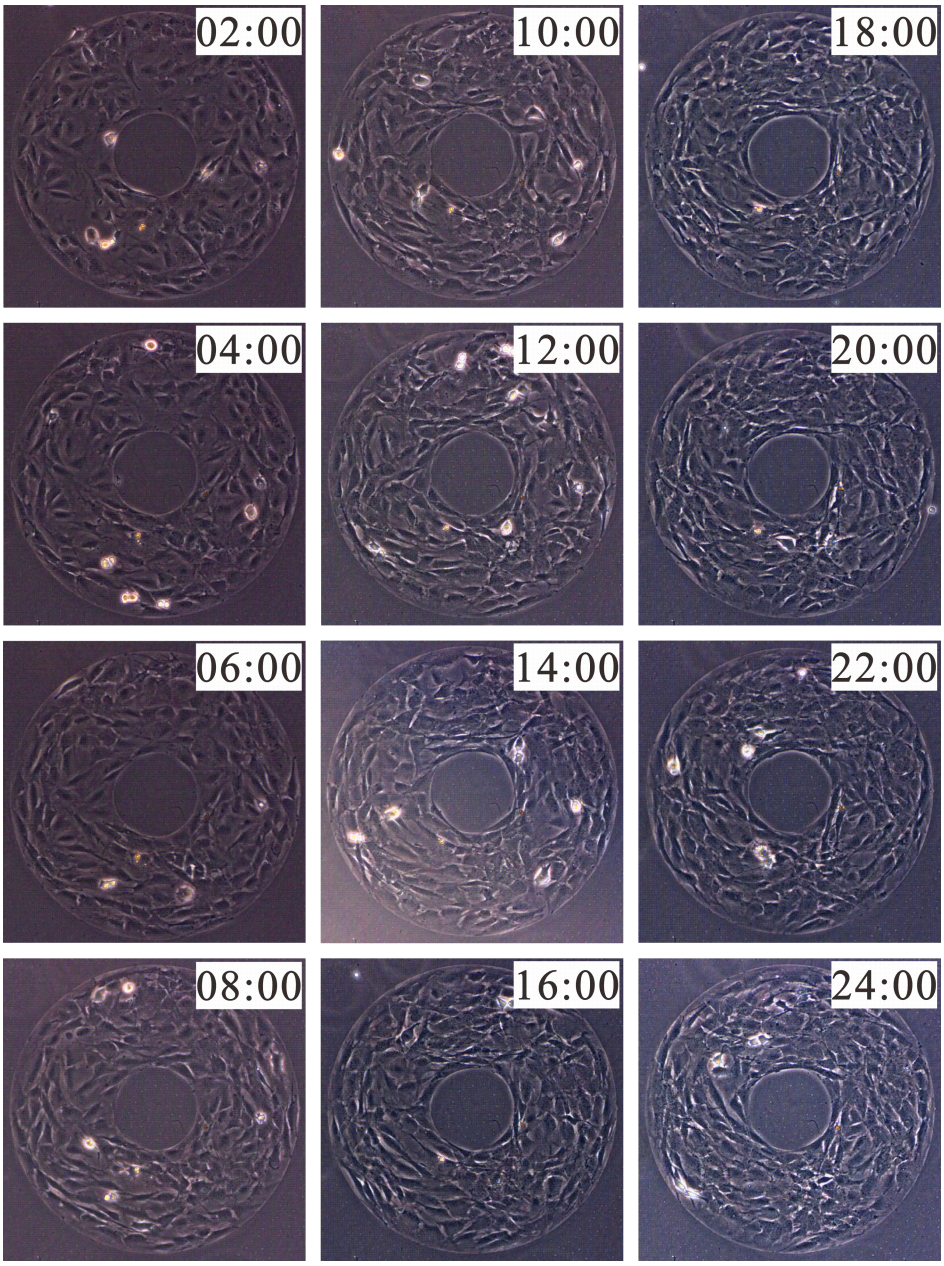

Figure S7. The snapshots of evolution of arrangement and polarization of osteoblasts on the ring pattern with inner radius of 100 μm over a period of 24 h.

S2. Coefficients C_1 and C_2 in Eq. 7 in the text

With boundary conditions Eq. 6, C_1 and C_2 can be determined as

$$C_1 = -\varepsilon_0 (1+\upsilon)\frac{C_{11}}{C_{10}+C_{12}}, C_2 = \varepsilon_0 (1+\upsilon)\frac{C_{22}}{C_{10}+C_{12}}. \qquad \text{(s2.1)}$$

where

$$\begin{aligned} C_{10} &= \left((\upsilon-1)\mathrm{K}_{11} - \alpha R_1 \mathrm{K}_{01}\right)\alpha R_0 \mathrm{I}_{00} + \left(\alpha R_0 \mathrm{K}_{00} + (1-\upsilon)\mathrm{K}_{10}\right)\alpha R_1 \mathrm{I}_{01} \\ C_{12} &= (1-\upsilon)\left[\left(\alpha R_1 \mathrm{K}_{01} + (1-\upsilon)\mathrm{K}_{11}\right)\mathrm{I}_{10} - \left(\alpha R_0 \mathrm{K}_{00} + (1-\upsilon)\mathrm{K}_{10}\right)\mathrm{I}_{11}\right], \\ C_{11} &= \alpha R_0 R_1 (\mathrm{K}_{00} - \mathrm{K}_{01}) + R_1 (1-\upsilon)\mathrm{K}_{10} + R_0 (\upsilon-1)\mathrm{K}_{11} \\ C_{22} &= \alpha R_0 R_1 (\mathrm{I}_{01} - \mathrm{I}_{00}) + R_1 (1-\upsilon)\mathrm{I}_{10} + R_0 (\upsilon-1)\mathrm{I}_{11} \end{aligned} \qquad \text{(s2.2)}$$

in which I_{00}=BesslI$(0,\alpha R_0)$, I_{10}=BesslI$(1,\alpha R_0)$, I_{01}=BesslI$(0,\alpha R_1)$, I_{11}=BesslI$(1,\alpha R_1)$, and

K_{00}=BesslK$(0,\alpha R_0)$, K_{10}=BesslK$(1,\alpha R_0)$, K_{01}=BesslK$(0,\alpha R_1)$, K_{11}=BesslK$(1,\alpha R_1)$.

S3. Orthotropic model of cell layer

Considering the effect of cell polarization along the circumferential direction, the cell layer is modeled as an orthotropic membrane with Young's modulus in radial direction E_r and that in circumferential direction E_θ. The plane stress constitutive relation for an axial symmetric problem of the orthotropic membrane in polar coordinate is written as

$$\begin{cases} \sigma_r = E_{rr}\varepsilon_r + E_{r\theta}\varepsilon_\theta + \left(E_{rr} + E_{r\theta}\right)\varepsilon_0 \\ \sigma_\theta = E_{r\theta}\varepsilon_r + E_{\theta\theta}\varepsilon_\theta + \left(E_{r\theta} + E_{\theta\theta}\right)\varepsilon_0 \end{cases} \quad \text{(s3.1)}$$

where

$$E_{rr} = \frac{E_r}{1-\mu_{r\theta}\mu_{\theta r}},\ E_{\theta\theta} = \frac{E_\theta}{1-\mu_{r\theta}\mu_{\theta r}},\ E_{r\theta} = \frac{\mu_{r\theta}E_\theta}{1-\mu_{r\theta}\mu_{\theta r}},\ \mu_{\theta r} = \frac{E_\theta\mu_{r\theta}}{E_r} \quad \text{(s3.2)}$$

Considering Eq. s3.1, 2 and 3, the equilibrium equation is obtained as

$$\frac{d^2u}{dr^2} + \frac{1}{r}\frac{du}{dr} - \frac{a^2}{r^2}u - b^2u + \frac{1-a^2}{r}\varepsilon_0 = 0 \quad \text{(s3.3)}$$

where $a = \sqrt{E_\theta / E_r}$, and $b = \sqrt{\rho k_{eff} / E_{rr} h_c}$. Solving Eq. s3.3, we obtain

$$u = C_3\mathrm{BesslI}\left(a,br\right) + C_4\mathrm{BesslK}\left(a,br\right) + f\left(r\right) \quad \text{(s3.4)}$$

where $f(r)$ is a particular solution. The constants C_3 and C_4 can be determined using the boundary conditions Eq. 6 in the main text, i.e. $\sigma_r = 0$ at $r = R_0$ and $r = R_1$. Substituting Eq. s3.4 into Eq. 2 and then Eq. s3.1, we obtain the radial and circumferential normal stresses σ_r and σ_θ, i.e., the in-plane minimum and maximum principle stresses as,

$$\sigma_r = \frac{1}{1-a^2\upsilon_{r\theta}^2}\left\{\begin{array}{l} \mathrm{C}_3E_r\left[\dfrac{\upsilon_{\theta r}+a}{r}\mathrm{BesslI}\left(a,br\right) + b\mathrm{BesslI}\left(a+1,br\right)\right] \\ +\mathrm{C}_4E_r\left[\dfrac{\upsilon_{\theta r}+a}{r}\mathrm{BesslK}\left(a,br\right) - b\mathrm{BesslK}\left(a+1,br\right)\right] \\ +\left(E_r + E_\theta\upsilon_{r\theta}\right)\varepsilon_0 + E_r\left(\dfrac{df\left(r\right)}{dr} + \dfrac{\upsilon_{\theta r}}{r}f\left(r\right)\right) \end{array}\right\} \quad \text{(s3.5)}$$

and

$$\sigma_\theta = \frac{1}{1-a^2\upsilon_{r\theta}^2}\left\{\begin{array}{l} \mathrm{C}_3 E_\theta\left[\dfrac{1+a\upsilon_{r\theta}}{r}\,\mathrm{BesslI}\left(a,br\right)+b\upsilon_{r\theta}\mathrm{BesslI}\left(a+1,br\right)\right] \\ +\mathrm{C}_4 E_\theta\left[\dfrac{1+a\upsilon_{r\theta}}{r}\,\mathrm{BesslK}\left(a,br\right)-\upsilon_{r\theta}b\mathrm{BesslK}\left(a+1,br\right)\right] \\ +\left(E_\theta\upsilon_{r\theta}+E_\theta\right)\varepsilon_0+E_\theta\left(\upsilon_{r\theta}\dfrac{df\left(r\right)}{dr}+\dfrac{f\left(r\right)}{r}\right) \end{array}\right\} \tag{s3.6}$$

thus, we obtain the in-plane maximum shear stress as

$$\bar{\tau}_{\max} = \frac{\sigma_\theta-\sigma_r}{2} = \frac{1}{2\left(1-\left(E_r/E_\theta\right)\upsilon_{r\theta}^2\right)}\left\{\begin{array}{l} \dfrac{E_r\left(\upsilon_{\theta r}a-\upsilon_{\theta r}-a\right)+E_\theta}{r}\left[\mathrm{C}_3\mathrm{BesslI}\left(a,br\right)+\mathrm{C}_4\mathrm{BesslK}\left(a,br\right)\right] \\ +bE_r\left(\upsilon_{\theta r}-1\right)\left[\mathrm{C}_3\mathrm{BesslI}\left(a+1,br\right)-\mathrm{C}_4\mathrm{BesslK}\left(a+1,br\right)\right] \\ +\left(E_\theta-E_r\right)\varepsilon_0+E_r\left(\upsilon_{\theta r}-1\right)\dfrac{df\left(r\right)}{dr}+E_\theta\left(1-\upsilon_{r\theta}\right)\dfrac{f\left(r\right)}{r} \end{array}\right\} \tag{s3.7}$$

Similarly, C_3 and C_4 can be determined as

$$C_3 = \frac{C_{33}}{C_{34}}, C_4 = \varepsilon_0\,\frac{C_{44}}{C_{34}}. \tag{s3.8}$$

where

$$\left\{\begin{array}{l} C_{34} = \left(\left(a+\upsilon_{\theta r}\right)\mathrm{K}_a^1-bR_1\mathrm{K}_{a+1}^1\right)\left(R_0\mathrm{I}_{a+1}^0+\dfrac{a+\upsilon_{\theta r}}{b}\mathrm{I}_a^0\right) \\ +\left(bR_0\mathrm{K}_{a+1}^0-\left(a+\upsilon_{r\theta}\right)\mathrm{K}_a^0\right)\left(R_1\mathrm{I}_{a+1}^1+\dfrac{a+\upsilon_{\theta r}}{b}\mathrm{I}_a^1\right) \\ \\ C_{33} = \left(a+\upsilon_{\theta r}+a\upsilon_{\theta r}+\upsilon_{\theta r}^2\right)b^{-1}\varepsilon_0\left(R_1\mathrm{K}_a^0-R_0\mathrm{K}_a^1\right)+b^{-1}\left(a+\upsilon_{\theta r}\right)\left(f_{R1}R_1\mathrm{K}_a^0-f_{R0}R_0\mathrm{K}_a^1\right) \\ +b^{-1}\upsilon_{\theta r}\left(a+\upsilon_{\theta r}\right)\left(f\left(R_1\right)\mathrm{K}_a^0-f\left(R_0\right)\mathrm{K}_a^1\right)-\varepsilon_0R_0R_1\left(1+\upsilon_{\theta r}\right)\left(\mathrm{K}_{a+1}^0-\mathrm{K}_{a+1}^1\right) \\ -R_0R_1\left(f_{R1}\mathrm{K}_{a+1}^0-f_{R0}\mathrm{K}_{a+1}^1\right)-\upsilon_{\theta r}\left(f\left(R_1\right)R_0\mathrm{K}_{a+1}^0-f\left(R_0\right)R_1\mathrm{K}_{a+1}^1\right) \\ \\ C_{44} = -\left(a+\upsilon_{\theta r}+a\upsilon_{\theta r}+\upsilon_{\theta r}^2\right)b^{-1}\varepsilon_0\left(R_1\mathrm{I}_a^0-R_0\mathrm{I}_a^1\right)-b^{-1}\left(a+\upsilon_{\theta r}\right)\left(f_{R1}R_1\mathrm{I}_a^0-f_{R0}R_0\mathrm{I}_a^1-\right) \\ -b^{-1}\upsilon_{\theta r}\left(a+\upsilon_{\theta r}\right)\left(f\left(R_1\right)\mathrm{I}_a^0-f\left(R_0\right)\mathrm{I}_a^1\right)-\varepsilon_0R_0R_1\left(1+\upsilon_{\theta r}\right)\left(\mathrm{I}_{a+1}^0-\mathrm{I}_{a+1}^1\right) \\ -R_0R_1\left(f_{R1}\mathrm{I}_{a+1}^0-f_{R0}\mathrm{I}_{a+1}^1\right)-\upsilon_{\theta r}\left(f\left(R_1\right)R_0\mathrm{I}_{a+1}^0-f\left(R_0\right)R_1\mathrm{I}_{a+1}^1\right) \end{array}\right. \tag{s3.9}$$

where $\mathrm{I}_a^0=\mathrm{BesslI}\left(a,bR_0\right)$, $\mathrm{I}_{a+1}^0=\mathrm{BesslI}\left(a+1,bR_0\right)$, $\mathrm{I}_a^1=\mathrm{BesslI}\left(a,bR_1\right)$, $\mathrm{I}_{a+1}^1=\mathrm{BesslI}\left(a+1,bR_1\right)$,

$\mathrm{K}_a^0=\mathrm{BesslK}\left(a,bR_0\right)$, $\mathrm{K}_{a+1}^0=\mathrm{BesslK}\left(a+1,bR_0\right)$, $\mathrm{K}_a^1=\mathrm{BesslK}\left(a,bR_1\right)$, $\mathrm{K}_{a+1}^1=\mathrm{BesslK}\left(a+1,bR_1\right)$

$$f_{R0}=\left.\frac{df(r)}{dr}\right|_{r=R_0} \quad \text{and} \quad f_{R1}=\left.\frac{df(r)}{dr}\right|_{r=R_1}.$$

The expression of the particular solution is

$$f(r)=-\frac{\varepsilon_0 r}{2a\sin(a\pi)\Gamma(a)}\left(\begin{array}{l} a(a+1)2^a b^{-a}\Gamma(a)^2\sin(a\pi)\,\text{BesselI}(a,br)\,r^{-a}\,\text{hypergeom}\left(\frac{1-a}{2},\left[1-a,\frac{3-a}{2}\right],4b^2r^2\right) \\ +(a-1)b^a\left[2^{-a}\pi\,\text{BesselI}(a,br)+2^{1-a}\sin(a\pi)\,\text{BesselK}(a,br)\right]r^a \\ \text{hypergeom}\left(\frac{1+a}{2},\left[1+a,\frac{3+a}{2}\right],4b^2r^2\right) \end{array}\right) \quad \text{(s3.10)}$$

where the functions "hypergeom" and "Γ" can calculated through commercial software MAPPLE. In the calculation, we set $E_\theta = 10kPa$ and $\mu_{\theta r}=0.45$, $\rho k_{eff}=0.00125\,nN/um^3$ in Fig. S8, and chose three value for E_θ/E_r as 1, 2 and 10/3 in our model (Fig. S8).

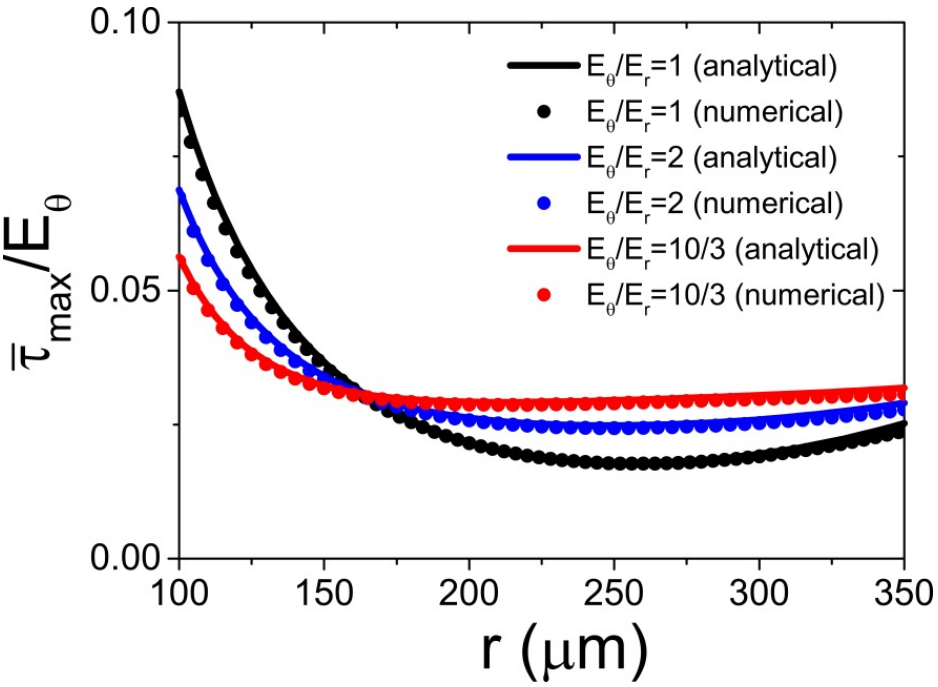

Figure S8. Predictions of the radial distribution of maximum shear stress using the orthotropic model. The numerical solutions are obtained through commercial software ABAQUS.